

Easy-IIL: Reducing Human Operational Burden in Interactive Imitation Learning via Assistant Experts

Chengjie Zhang^{1,2}, Chao Tang³, Wenlong Dong^{1,2}, Dehao Huang^{1,2}, Aoxiang Gu^{1,2},
and Hong Zhang^{1,2} *Life Fellow, IEEE*

Abstract—Interactive Imitation Learning (IIL) typically relies on extensive human involvement for both offline demonstration and online interaction. Prior work primarily focuses on reducing human effort in passive monitoring rather than active operation. Interestingly, structured model-based imitation approaches achieve comparable performance with significantly fewer demonstrations than end-to-end imitation learning policies in the low-data regime. However, these methods are typically surpassed by end-to-end policies as the data increases. Leveraging this insight, we propose Easy-IIL, a framework that utilizes off-the-shelf model-based imitation methods as an assistant expert to replace active human operation for the majority of data collection. The human expert only provides a single demonstration to initialize the assistant expert and intervenes in critical states where the task is approaching failure. Furthermore, Easy-IIL can maintain IIL performance by preserving both offline and online data quality. Extensive simulation and real-world experiments demonstrate that Easy-IIL significantly reduces human operational burden while maintaining performance comparable to mainstream IIL baselines. User studies further confirm that Easy-IIL reduces subjective workload on the human expert. Project page: <https://sites.google.com/view/easy-iil>

I. INTRODUCTION

Imitation learning (IL) constitutes a paradigm for acquiring skills through the observation of expert demonstrations [1]. Building on this, Interactive Imitation Learning (IIL) [2] further enhances sample efficiency by introducing online interaction, which allows an expert to correct the compounding errors during policy rollouts. This has been validated across various domains, such as virtual games [3], autonomous driving [4], and robotic manipulation [5]. Standard IIL, as shown in Fig. 1(a), trains a novice from an expert-collected (a human in our case) offline dataset and then iterates online rollout, expert intervention at near-failure states, data aggregation, and retraining [2]. However, such a framework places a heavy burden on the human expert, limiting scalability as dataset size and task complexity grow and potentially inducing fatigue that degrades the quality of collected data.

To address the above challenge, prior work reduces the burden of *passive* human monitoring by developing real-time anomaly detection to inform when human intervention

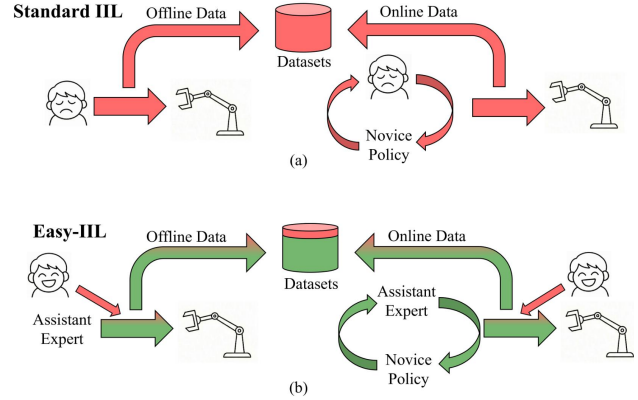


Fig. 1: (a) illustrates the standard IIL interaction mechanism, where a human expert is involved in both offline and online stages. (b) depicts Easy-IIL, which delegates most offline and online data collection and interactions to an assistant expert, substantially reducing active human operational effort.

is needed [4], [6], [7]. In this work, we push further toward reducing the *active* operational burden, the effort required to teleoperate the robot during both offline and online stages, while preserving IIL performance. Interestingly, recent model-based imitation methods [8]–[11] can perform robotic manipulation tasks from one or a few human demonstrations by leveraging generalizable priors from pre-trained models. Although these methods perform competitively in the low-data regime, they are typically surpassed by end-to-end IL policies at larger dataset scales.

Motivated by this observation, this paper introduces Easy-IIL, an IIL framework for robotic manipulation that utilizes off-the-shelf model-based imitation methods as an assistant expert to replace a human expert in the majority of the data collection process in both offline and online stages. Fig. 1(b) illustrates the conceptual pipeline of Easy-IIL. Specifically, the human expert only collects a single offline demonstration to initialize the assistant expert and perform intervention when the task is approaching failure. Furthermore, our data collection strategy guarantees that Easy-IIL’s performance is comparable to established IIL frameworks by maintaining both offline and online data quality. Simulations and real-world experiments demonstrate that Easy-IIL reduces human operational burden by 4–5 times compared to standard IIL, while maintaining comparable performance. Furthermore, user studies validate that the subjective workload is significantly reduced compared to the baselines.

¹Shenzhen Key Laboratory of Robotics and Computer Vision, Southern University of Science and Technology, Shenzhen, China.

²Department of Electronic and Electrical Engineering, Southern University of Science and Technology, Shenzhen, China.

³Department of Robotics, Perception, and Learning, KTH Royal Institute of Technology, Stockholm, Sweden.

This work was supported in part by the Shenzhen Key Laboratory of Robotics and Computer Vision (ZDSYS20220330160557001).

In brief, the contributions of this paper are organized as follows.

- We propose Easy-IIL, a novel IIL framework designed to minimize human operational effort by utilizing an assistant expert to replace the human in the majority of data collection while maintaining IIL performance.
- Extensive simulations, real-world experiments, and user studies are performed to demonstrate the effectiveness of the proposed Easy-IIL.

II. RELATED WORKS

A. Interactive Imitation Learning

Many IIL studies alleviate the human monitoring burden by designing real-time anomaly detectors to autonomously decide when intervention is needed, thereby framing the problem as a binary classification task. SafeDAgger [4], EnsembleDAgger [12], and HG-DAgger [6] utilize the safety metric for this decision, while ThriftyDAgger [13] and Liu et al. [7] employ two metrics: novelty and risk. More recently, Diff-DAgger [14] introduces the diffusion loss as the anomaly detection metric in the diffusion policy [15] to determine when to ask the human expert for help. Our framework complements these methods, but since minimizing monitoring effort is not our focus, we utilize human monitoring.

Some existing IIL works focus on enhancing IIL performance. For instance, IWR [16] splits online data into non-intervention and intervention subsets and re-weights them. Later studies, such as CEILING [17] and Sirius [5], further categorize the online data and apply corresponding weights to further improve policy performance. Luo et al. [18] reformulate IIL as reinforcement learning (RL), which offers a higher theoretical performance upper bound but demands a large volume of intervention data or significant training time. More recently, MILE [19] employs a mental model to mimic human intervention. However, MILE requires extensive intervention data to train this mental model and prior access to the action distribution of the intervention agent (typically human), which is impractical for real-world deployment. Compared with these works [5], [6], [16], our Easy-IIL significantly reduces human operational burden without compromising performance.

B. Imitation from Human Demonstrations.

These methods are model-based, leveraging rules to utilize pre-trained vision models for computing the spatial object relationship (typically the 6D pose) between the current observation and the demonstration. These relationships are then used to transfer the trajectory in demonstration for task execution [20], [21]. These works have adopted pre-trained vision foundation models to further enhance robotic manipulation performance [8], [9], [22], [23]. Recently, MimicFunc [24] introduces efficient strategies to generate offline real-world data for training end-to-end IL policies. We select some of them to form our assistant expert.

C. Data Generation for Imitation Learning

These studies generate a large number of demonstrations from a few human demonstrations. Methods like MimicGen [25], SkillGen [26], and CyberDemo [27] leverage human demonstrations and privileged information (inaccessible in the real world) from simulation to generate demonstrations with diverse initial conditions. However, they focus solely on offline data and suffer from sim-to-real gaps. Recent Real2Sim2Real work [28] trains IL policies by reconstructing real-world objects and recording their motion in simulation to generate extensive demonstrations. However, this method heavily relies on the quality of 3D reconstruction and object tracking. DemoGen [29] requires only one human demonstration to generate demonstrations in the real world. However, it remains limited to offline data generation and only supports the training of a policy whose input type is point cloud. Our work collects both offline and online data directly in the real world, eliminating sim-to-real or reconstruction gaps and supporting policies with diverse types of visual inputs.

III. METHOD

A. Overall Workflow

Easy-IIL begins with an offline phase. Initially, a human expert collects a single demonstration of a manipulation task to initialize both an assistant expert and a dataset. Subsequently, the assistant expert collects the remaining demonstrations and adds them to the dataset, with human intervention occurring only when the task is on the verge of failure. Then, the dataset is used to train an end-to-end imitation learning policy, yielding a novice policy.

This is followed by an online iteration phase. The novice policy is deployed to perform the manipulation task. During this phase, the assistant expert randomly intervenes in the novice policy’s execution, while the human intervenes only to prevent imminent failure. The online intervention data from both experts are then incorporated into the dataset to further improve the novice policy.

The pseudo-code for the overall Easy-IIL workflow is provided in Algorithm 1. Specifically, `ACTIVATE(·)` refers to the initialization of an assistant expert, while `DEPLOY(·)` implements the data collection strategy where the labels `ONE_DEMO`, `REST_DEMO`, and `CORRECTION` are used to represent the collection of the first offline demonstration, the remaining offline demonstrations, and the online intervention data respectively. Finally, `TRAIN(·)` executes the training process.

B. Data Collection Strategy

1) *Offline Data Collection:* In the offline phase, a human expert provides a single demonstration to initialize an assistant expert, which also serves as a dataset. Once initialized, the assistant expert acquires the ability to complete the task independently and is utilized to generate the remaining offline demonstrations. The human expert monitors this generation process, intervening only upon task anomalies. Let x_k , o_k , and a_k denote the state, observation, and action

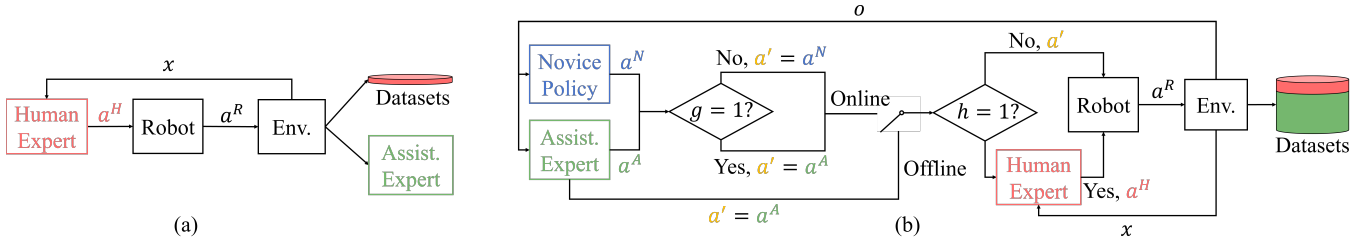


Fig. 2: Data collection strategy in Easy-IIL for (a) the first one offline demonstration and (b) the remaining offline demonstrations (“Offline” mode) and online interaction data (“Online” mode). Specifically, $a^H = \pi^H(s)$, $a^R = \pi^R(s)$, $a^A = \pi^A(o)$, $a^N = \pi^N(s)$. s and o represent state and observation, respectively.

at time step k , respectively [30]. Specifically, the state represents human perception input, whereas the observation corresponds to sensor readings [6]. Let π_0^R denote the robot policy controlling the robotic arm during the offline stage, defined as:

$$\pi_0^R(x_k) = h(k)\pi^H(x_k) + (1 - h(k))\pi^A(o_k) \quad (1)$$

where π^H and π^A represent the human expert and assistant expert policies, respectively. The term $h(k)$ serves as a gating function, whether the human takes control of the robot at k :

$$h(k) = \begin{cases} 1, & \text{human intervenes.} \\ 0, & \text{otherwise.} \end{cases} \quad (2)$$

The offline dataset where data are generated by π^H and π^A is defined as $\mathcal{D}^{off} = \{(o, a) | a \in \{\pi^H(x), \pi^A(o)\}\}$ and $\mathcal{D}^{off} = \mathcal{D}^{done} \cup \mathcal{D}^{rest}$, where \mathcal{D}^{done} and \mathcal{D}^{rest} are declared in Algorithm 1. Upon the completion of data collection, \mathcal{D}^{off} is utilized to train an end-to-end imitation learning policy. This yields a novice policy π_0^N , which initially exhibits low success rates and produces suboptimal actions. The offline data collection process is illustrated in Fig. 2(a) and Fig. 2(b) with “Offline” mode.

2) *Online Data Collection*: The online stage is divided into M rounds. In the i -th round ($i = 1, \dots, M$), a gating function $g_i(j, k)$ selects a sequence of actions (action chunk) from the novice policy π_{i-1}^N or the assistant expert π^A randomly. Simultaneously, a human expert monitors the execution, providing intervention actions exclusively upon near task failure. The human gating function $h(k)$ has been defined in Eq. (2). Therefore, the robot policy in the i -th round π_i^R is defined as follows:

$$\pi_i^R(x_k) = h(k)\pi^H(x_k) + (1 - h(k))[g_i(j, k)\pi^A(o_k) + (1 - g_i(j, k))\pi_{i-1}^N(o_k)]. \quad (3)$$

The definition of $g_i(j, k)$ is shown below,

$$g_i(j, k) = \begin{cases} 1, & X_j < \beta_i \text{ or } x_k \in \mathcal{B} \\ 0, & \text{otherwise} \end{cases} \quad (4)$$

where $\beta_i = \beta^i$ and β is defined manually. At the beginning, $j = 0$ and $k = 0$. Once an action is executed, $k = k + 1$; if an action is executed without human expert intervention,

$j = j + 1$. Specifically, X_j is defined below,

$$X_j = \begin{cases} Y, & \text{mod}(j, H) = 0. \\ X_{j-1}, & \text{otherwise.} \end{cases} \quad (5)$$

where $Y \sim \mathcal{U}(0, 1)$ and $\text{mod}(j, H)$ equals to the remainder of j divided by H (action chunk size). Compared to single action switching [3], the action chunk switching we used is better suited to end-to-end chunk-based policies, such as diffusion policy and ACT [31]. To enhance exploration for better online action quality, we add zero-mean Gaussian noise with standard deviation σ to the normalized novice policy actions with range $[-1, 1]$. Following [22], [26], [29], the manipulation workspace is divided into free space \mathcal{F} and bottleneck space \mathcal{B} . \mathcal{F} consists of an open area without obstacles, while \mathcal{B} refers to a region near or in contact with the target object. Since a robot approaching a target object at a closer range requires higher action precision, it is easier to fail in \mathcal{B} , especially for novice policy actions due to their low quality. Therefore, we disable the execution of novice policy actions within \mathcal{B} , which is implemented by Eq. (4) with $x_k \in \mathcal{B}$.

The online dataset where data are generated by π^H and π^A is defined as $\mathcal{D}^{on} = \{(o, a) | a \in \{\pi^H(x), \pi^A(o), \pi^N(o)\}\}$ and $\mathcal{D}^{on} = \mathcal{D}^{corr1} \cup \mathcal{D}^{corr2} \dots \cup \mathcal{D}^{corrM}$, where \mathcal{D}^{corr_i} ($i = 1, \dots, M$) is declared in Algorithm 1. Note that the weight of online data generated by the novice policy is set to 0, as detailed in Section III.C.2. After online data collection is completed in the i -th round, $\mathcal{D} = \mathcal{D}^{off} \cup \mathcal{D}^{on}$ is used to train π_{i-1}^N , as shown in Algorithm 1. The online data collection process is illustrated in Fig. 2(b) with “Online” mode. The data collection strategy corresponding to $\text{DEPLOY}(\cdot)$ is shown in Appendix B.

C. Implementation Details

1) *Assistant Expert*: We build upon these works [8], [22] as our assistant expert to achieve one-shot multi-stage robotic manipulation. For initialization, a human expert collects a single offline demonstration where each waypoint consists of an RGB-D image and the corresponding 6D end-effector (EE) pose and 1D gripper value. After initialization, the assistant expert takes the current RGB-D observation as input. Then, Grounded-SAM [32], and image matching techniques (SuperPoint [33] and LightGlue [34]) are employed to process RGB-D images from both the demonstration and the

Algorithm 1 Easy-III

Require: Rounds M , Offline Demonstration Number N_0 , Demonstration Number in the i -th Online Round N_i , Data Weights \mathcal{W} .
 $\mathcal{D} \leftarrow \emptyset, \mathcal{W} \leftarrow \emptyset$.
 Label = *ONE_DEMO* ▷ One Human Demo
 $\mathcal{D}^{one}, \mathcal{W}^{one} \leftarrow \text{DEPLOY}(\pi^H, \text{None}, \text{None}, 1, \text{Label}, \text{None})$
 $\mathcal{D} \leftarrow \mathcal{D}^{one}, \mathcal{W} \leftarrow \mathcal{W}^{one}$
 $\pi^A \leftarrow \text{ACTIVATE}(\mathcal{D})$

Label = *REST_DEMO* ▷ Rest Offline Demos
 $\mathcal{D}^{rest}, \mathcal{W}^{rest} \leftarrow \text{DEPLOY}(\pi^H, \pi^A, \text{None}, N_0 - 1, \text{Label}, \text{None})$
 $\mathcal{D} \leftarrow \mathcal{D} \cup \mathcal{D}^{rest}, \mathcal{W} \leftarrow \mathcal{W} \cup \mathcal{W}^{rest}$
 $\pi_0^N \leftarrow \text{TRAIN}(\mathcal{D}, \mathcal{W}, \text{None})$

Label = *CORRECTION* ▷ Online Corrections
for $i = 1, 2, \dots, M$ **do**
 $\beta_i \leftarrow \beta^i$
 $\mathcal{D}^{corr_i}, \mathcal{W}^{corr_i} \leftarrow \text{DEPLOY}(\pi^H, \pi^A, \pi_{i-1}^N, N_i, \text{Label}, \beta_i)$
 $\mathcal{D} \leftarrow \mathcal{D} \cup \mathcal{D}^{corr_i}, \mathcal{W} \leftarrow \mathcal{W} \cup \mathcal{W}^{corr_i}$
 $\pi_i^N \leftarrow \text{TRAIN}(\mathcal{D}, \mathcal{W}, \pi_{i-1}^N)$
end for
return π_M^N

input, thereby extracting a pair of target object point clouds with established correspondences. Subsequently, the 6D pose transformation is computed via Iterative Closest Point (ICP) [35] and RANSAC [36]. Within the demonstration trajectory, the 6D poses are transformed using this transformation, while the gripper values remain unchanged, resulting in the transformed trajectory. After that, the transformed trajectory in \mathcal{F} is re-planned using linear interpolation for positions and Spherical Linear Interpolation (Slerp) [37] for orientations, while the gripper values remain the same. The output is the first unvisited waypoint in the transformed trajectory to be executed.

A recovery behavior is triggered whenever the 6D pose deviation from the transformed trajectory exceeds a predefined threshold. A new transformed trajectory is generated via the replanning mentioned above, targeting the first unvisited waypoint within \mathcal{B} .

2) *Training Details:* We employ a diffusion policy as our end-to-end chunk-based IL policy. The training process utilizes the DDPM noise scheduler [38], with Mean Squared Error (MSE) serving as the loss function. The training loss [15] is formulated as follows,

$$\mathcal{L} := \mathbb{E}_{a_{k:k+Hp-1}^0, o_k, n, \epsilon} [\|\epsilon - \epsilon_\theta(a_{k:k+Hp-1}^n, o_k, n)\|_2^2] \quad (6)$$

where $\epsilon \sim \mathcal{N}(\mathbf{0}, \mathbf{1})$ is the standard Gaussian noise, $\epsilon_\theta(\cdot)$ is the noise prediction model, $a_{k:k+Hp-1}^0$ represents the clean action chunk, $a_{k:k+Hp-1}^n$ represents the noisy action chunk at the n -th scheduling step ($n > 0$), and Hp means the action chunk size for prediction.

We define a weight matrix W_k associated with an action chunk, where each row corresponds to an action. The weighting rule depends on the action’s source: the row is set to $\mathbf{0}$ if the action is generated by the novice policy, and to $\mathbf{1}$ if generated by the human or assistant expert. Consequently,

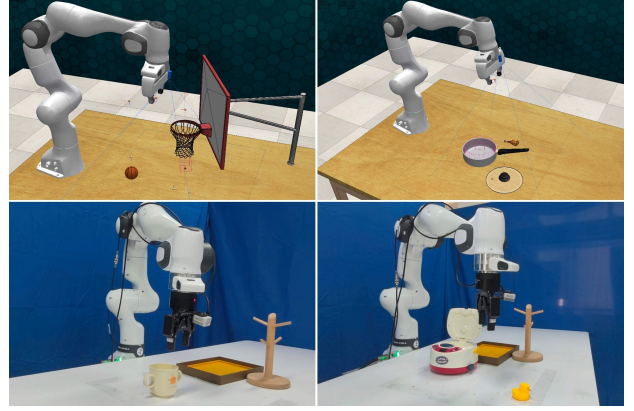


Fig. 3: Four task scenarios. Basketball in Hoop (left-top), Take Chicken in Saucepan (right-top), Hang the Cup (left-bottom), Put Duck in Cooker (right-bottom).

the weighted training loss is formulated as:

$$\mathcal{L} := \mathbb{E}_{a_{k:k+Hp-1}^0, o_k, n, \epsilon} [\|W_k \otimes (\epsilon - \epsilon_\theta(a_{k:k+Hp-1}^n, o_k, n))\|_2^2]. \quad (7)$$

Note that for training, we only utilize samples whose first action in the action chunk originates from either the assistant expert or the human expert. The detailed training hyperparameters are provided in Table VI in Appendix A.

IV. EXPERIMENTS

Our evaluation comprises main experiments, ablation studies, additional experiments, and a user study. The main experiments demonstrate that Easy-III effectively reduces human operational effort while maintaining IIL performance. The ablation studies validate Easy-III’s effectiveness in both offline and online stages. Furthermore, additional experiments are conducted to verify: 1) the end-to-end IL policy trained via Easy-III achieves a higher performance upper bound than the model-based assistant expert; and 2) the specific impact of the random-switching mechanism for action chunks. Finally, the user study demonstrates that Easy-III achieves a significant reduction in subjective operational workload.

A. Tasks

Simulations: Our simulations are conducted in RL Bench [39], featuring both an existing two-stage task and a custom long-horizon four-stage task. The two-stage task, “Basketball in Hoop”, involves picking up a basketball and placing it in a hoop. The custom-designed four-stage task, “Take Chicken in Saucepan”, requires picking up a chicken, placing it in a saucepan, retrieving the lid, and covering the pan. The simulated task scenes are shown in the top two panels of Fig. 3. A human controls the four degrees of freedom (3D position and 1D gripper) of the end-effector via a keyboard.

Real-World Experiments: We set up two manipulation tasks. The first is a two-stage task named “Hang the Cup”, which involves grasping a cup and hanging it on a holder. The second is a three-stage task, “Put Duck in Cooker”, which requires picking up a toy duck, placing it into a

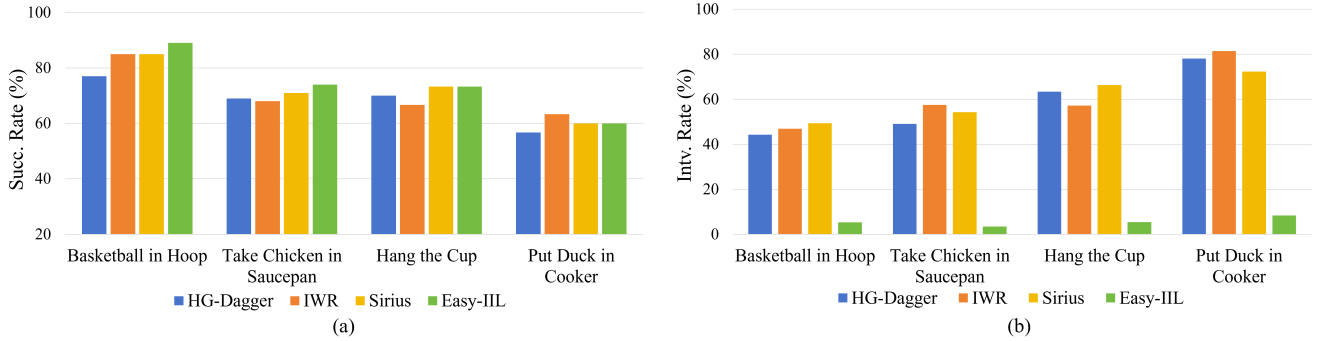


Fig. 4: Main experiment results evaluating Succ. Rate (a) and Intv. Rate (b) across four tasks for Easy-IIL, HG-Dagger, IWR, and Sirius. Easy-IIL is configured with $H = 8$ and $\sigma = 0.3$.

cooker, and closing the cooker. The real-world task scenes are illustrated in the bottom two panels of Fig. 3.

The real-world experiments utilize a Franka Research 3 robotic arm, with the Gello [40] serving as a teleoperation interface. A human expert teleoperates the robotic arm by controlling the Gello, facilitated by a direct joint-to-joint mapping.

B. Baselines and Metrics

1) *Baselines*: Three mainstream IIL methods—HG-Dagger, IWR, and Sirius—are employed as baselines. These baselines follow the standard IIL framework (introduced in the first paragraph of Section I) for data collection. To ensure good performance, we fine-tune the parameters for IWR and Sirius.

2) *Metrics*: For the main, ablation, and additional experiments, we evaluate the IIL performance using the task Success Rate (Succ. Rate), defined as the rate at which the trained end-to-end policy successfully executes the assigned task. Also, we evaluate human operational burden by human intervention rate (Intv. Rate). Intv. Rate is a variant of the normalized Return On Human Effort (ROHE) [7], [41], modified to retain only the denominator term, thereby allowing for the direct quantification of human operational burden. The intervention rate is expressed as follows:

$$\text{Intv. Rate} = \frac{N^H}{N} \times 100\% \quad (8)$$

where N^H represents the number of human actions and N means the total number of actions.

For the user study, we employ the Raw-TLX [42] (unweighted NASA-TLX [43]) and retain three key metrics: Performance, Effort, and Frustration. The users rate each metric on a 7-point Likert scale (1 = Lowest, 7 = Highest). The definitions for these metrics are as follows:

- **Performance (P)**: Reflects the user’s satisfaction with the operation results. A higher score indicates a higher level of satisfaction.
- **Effort (E)**: Measure the amount of mental and physical effort exerted by the user when teleoperating the robotic arm.
- **Frustration (F)**: Assess the level of impatience, insecurity, or annoyance experienced during operation.

The Burden, derived from the three metrics, is defined as:

$$\text{Burden} = \frac{(7 - P) + E + F}{3}. \quad (9)$$

Note that the Burden score is a simplified version of the Raw-TLX score, as we select three key metrics from the original six for computation. We employ the Wilcoxon Signed-Rank Test [44] to conduct a significance test on the subjective operational burden between Easy-IIL and IIL baselines.

C. Experiment Details

The main experiment, ablation studies, the second part of additional experiments, and the user study require 10 offline demonstrations and 4 online rounds, with 5 interactive trajectories per round (50 demonstrations). In the first part of the additional experiments, we increase the dataset size to 10 offline demonstrations and 8 online rounds, each containing 5 interactive trajectories (80 demonstrations).

The main experiment comprises two simulated tasks performed by 10 participants (aged 20–27) using a fixed random seed, along with two real-world tasks conducted by a single participant over three trials. The ablation and additional experiments focus on two simulated tasks, involving a single participant across three different random seeds. For the user study, 10 participants provided ratings based on the entire operation process of the two simulation tasks.

In the simulation, we evaluate 60 trajectories per checkpoint for each seed to compute the success rate, reporting the average across all seeds. We select the best one from the six checkpoints as the reported success rate. For real-world experiments, we evaluate 30 trajectories per trial (with one checkpoint each) and report the mean success rate across all trials.

Note that “Basketball” and “Chicken” refer to the Basketball in Hoop and Take Chicken in Saucepan tasks, respectively, in Tables I, II, III, IV, and V.

D. Experiment Results

1) *Main Results*: Fig. 4(a) demonstrates that Easy-IIL consistently achieves performance comparable to all IIL baselines, with success rate differences within a 3-4% margin. As shown in Fig. 4(b), Easy-IIL significantly reduces

the human intervention rate across all tasks, achieving a substantial four- to five-fold reduction. These results verify the effectiveness of Easy-IIL.

2) *Ablation Results:* As illustrated in Table I, across the two simulated tasks, the offline Succ. Rate of Easy-IIL is comparable to that of the baselines. The offline Intv. The rate of Easy-IIL is substantially lower than that of baselines. These results confirm the effectiveness of Easy-IIL in the offline stage. Note that the offline stage is identical across all baselines.

TABLE I: Ablation study results evaluating Succ. Rate and Intv. Rate across two simulated tasks for Baselines and Easy-IIL

Task	Succ. Rate (%) \uparrow		Intv. Rate (%) \downarrow	
	Baselines	Easy-IIL	Baselines	Easy-IIL
Basketball	74.3	78.0	100.0	4.6
Chicken	68.3	65.0	100.0	2.8

Fig. 5(a) illustrates that for both simulation tasks, incorporating action chunk switching (Ours vs. w/o Chunk), injecting noise into novice policy actions (Ours vs. w/o Noise), and disabling novice actions in \mathcal{B} (Ours vs. w/o Prohibition) contribute to a higher Succ. Rate. Additionally, Fig. 5(b) shows that disabling novice actions in \mathcal{B} significantly reduces human online intervention across both tasks. These results confirm the effectiveness of Easy-IIL in the online stage.

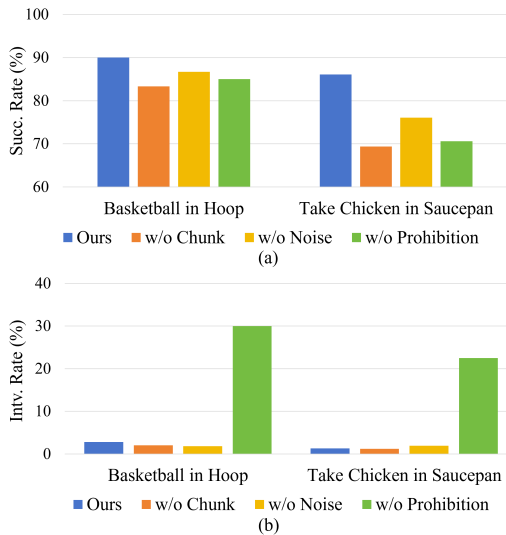


Fig. 5: Ablation studies results evaluating (a) Succ. Rate and (b) Intv. Rate across two simulated tasks for online strategy of Easy-IIL. Easy-IIL is configured with $H = 8$ and $\sigma = 0.3$.

We investigate the sensitivity of IIL performance to the variations of parameters (H and σ) in Easy-IIL’s online strategy, as detailed in Table II. It can be observed that the Succ. Rate remains stable within a 3% margin as parameters vary, underscoring the robustness of Easy-IIL’s online strategy against parameter variations.

TABLE II: Ablation study results evaluating Succ. Rate across two simulated tasks for parameter variations in the online strategy of Easy-IIL. Top: varying H (with $\sigma = 0.3$); Bottom: varying σ (with $H = 8$).

Succ. Rate (%)	$H = 4$	$H = 8$	$H = 12$
Basketball	90.0	90.0	88.9
Chicken	84.4	86.1	83.3

Succ. Rate (%)	$\sigma = 0.2$	$\sigma = 0.3$	$\sigma = 0.4$
Basketball	88.3	90.0	88.9
Chicken	84.4	86.1	83.9

3) *Additional Results:* For the first part, Table III shows that as the amount of data increases, the end-to-end IIL policy outperforms the model-based assistant expert with handcrafted rules. Note that assignments of 50 and 80 demonstrations are mentioned in the first paragraph of Section IV.C.

TABLE III: The first part of the additional experiment results evaluating Succ. Rate for assistant expert (Assist. Expert), diffusion policy trained via Easy-IIL with 50 demonstrations (DP-50demos), and 80 demonstrations (DP-80demos).

Succ. Rate (%)	Assist. Expert	DP-50demos	DP-80demos
Basketball	91.7	90.0	95.0
Chicken	88.9	86.1	91.7

For the second part, Table IV shows that action chunk switching increases the Succ. Rate of BC-RNN, whose architecture is CNN-LSTM-GMM, provides no benefit for CNN-GMM. This observation, consistent with the improvements shown in Fig. 5a, suggests that action chunk switching is beneficial for sequence-based policies, including chunk-based (diffusion policy) and auto-regressive (BC-RNN), but yields no performance gain for policies with single input and single output (CNN-GMM).

TABLE IV: The second part of the additional experiment results evaluating Succ. Rate of BC-RNN and CNN-GMM with ($H = 8$) and without ($H = 1$) action chunk switching across two simulated tasks.

Succ. Rate (%)	BC-RNN		CNN-GMM	
	H=1	H=8	H=1	H=8
Basketball	48.9	56.7	47.8	45.0
Chicken	57.8	65.0	31.1	34.4

4) *User Study Results:* Table V indicates that Easy-IIL achieves a statistically significant reduction in subjective operational workload across the two simulation tasks when compared to IIL baselines.

TABLE V: User study results evaluating Burden for Baselines and Easy-IIL. HG-Dagger, IWR, and Sirius are grouped as the Baselines. Burden are presented as Mean \pm Standard Deviation.

Burden	Baselines	Easy-IIL	p -value
Basketball	4.0 ± 0.6	1.7 ± 0.8	< 0.01
Chicken	5.0 ± 0.8	2.3 ± 0.9	< 0.01

V. CONCLUSIONS

We propose Easy-IIL, an IIL framework that significantly reduces the human operational burden while maintaining comparable performance. Easy-IIL leverages an off-the-shelf assistant expert to replace the majority of human operations during data collection. The human expert is only required to collect a single offline demonstration to initialize the assistant expert and to intervene in cases of near-failure. Easy-IIL preserves both offline and online data quality to keep IIL performance. Extensive simulation and real-world experiments demonstrate the effectiveness of Easy-IIL. Additionally, a user study confirms that Easy-IIL substantially lowers subjective operational workload.

REFERENCES

- [1] T. Zhang, Z. McCarthy, O. Jow, D. Lee, X. Chen, K. Goldberg, and P. Abbeel, "Deep imitation learning for complex manipulation tasks from virtual reality teleoperation," in *2018 IEEE International Conference on Robotics and Automation (ICRA)*, 2018, pp. 5628–5635.
- [2] C. Celemin, R. Pérez-Dattari, E. Chisari, G. Franzese, L. de Souza Rosa, R. Prakash, Z. Ajanović, M. Ferraz, A. Valada, and J. Kober, 2022.
- [3] S. Ross, G. Gordon, and D. Bagnell, "A reduction of imitation learning and structured prediction to no-regret online learning," in *Proceedings of the fourteenth international conference on artificial intelligence and statistics*. JMLR Workshop and Conference Proceedings, 2011, pp. 627–635.
- [4] J. Zhang and K. Cho, "Query-efficient imitation learning for end-to-end simulated driving," in *Proceedings of the AAAI conference on artificial intelligence*, vol. 31, no. 1, 2017.
- [5] H. Liu, S. Nasiriany, L. Zhang, Z. Bao, and Y. Zhu, "Robot learning on the job: Human-in-the-loop autonomy and learning during deployment," *The International Journal of Robotics Research*, p. 02783649241273901, 2022.
- [6] M. Kelly, C. Sidrane, K. Driggs-Campbell, and M. J. Kochenderfer, "Hg-dagger: Interactive imitation learning with human experts," in *2019 International Conference on Robotics and Automation (ICRA)*, 2019, pp. 8077–8083.
- [7] H. Liu, S. Dass, R. Martín-Martín, and Y. Zhu, "Model-based runtime monitoring with interactive imitation learning," in *2024 IEEE International Conference on Robotics and Automation (ICRA)*, 2024, pp. 4154–4161.
- [8] N. Di Palo and E. Johns, "Dinobot: Robot manipulation via retrieval and alignment with vision foundation models," in *2024 IEEE International Conference on Robotics and Automation (ICRA)*, 2024, pp. 2798–2805.
- [9] C. Tang, A. Xiao, Y. Deng, T. Hu, W. Dong, H. Zhang, D. Hsu, and H. Zhang, "Functo: Function-centric one-shot imitation learning for tool manipulation," *arXiv preprint arXiv:2502.11744*, 2025.
- [10] Y. Wang and E. Johns, "One-shot dual-arm imitation learning," *arXiv preprint arXiv:2503.06831*, 2025.
- [11] Y. Cai, J. Gao, C. Pohl, and T. Asfour, "Visual imitation learning of task-oriented object grasping and rearrangement," in *2024 IEEE/RSJ International Conference on Intelligent Robots and Systems (IROS)*. IEEE, 2024, pp. 364–371.
- [12] K. Menda, K. Driggs-Campbell, and M. J. Kochenderfer, "Ensembledagger: A bayesian approach to safe imitation learning," in *2019 IEEE/RSJ International Conference on Intelligent Robots and Systems (IROS)*, 2019, pp. 5041–5048.
- [13] R. Hoque, A. Balakrishna, E. R. Novoseller, A. Wilcox, D. S. Brown, and K. Goldberg, "Thriftydagger: Budget-aware novelty and risk gating for interactive imitation learning," in *Conference on Robot Learning (CoRL)*, 2021, pp. 598–608. [Online]. Available: <https://proceedings.mlr.press/v164/hoque22a.html>
- [14] S.-W. Lee and Y.-L. Kuo, "Diff-dagger: Uncertainty estimation with diffusion policy for robotic manipulation," in *CoRL 2024 Workshop on Mastering Robot Manipulation in a World of Abundant Data*.
- [15] C. Chi, Z. Xu, S. Feng, E. Cousineau, Y. Du, B. Burchfiel, R. Tedrake, and S. Song, "Diffusion policy: Visuomotor policy learning via action diffusion," *The International Journal of Robotics Research*, p. 02783649241273668, 2023.
- [16] A. Mandlkar, D. Xu, R. Martín-Martín, Y. Zhu, L. Fei-Fei, and S. Savarese, "Human-in-the-loop imitation learning using remote teleoperation," *arXiv preprint arXiv:2012.06733*, 2020.
- [17] E. Chisari, T. Welschehold, J. Boedecker, W. Burgard, and A. Valada, "Correct me if i am wrong: Interactive learning for robotic manipulation," *IEEE Robotics and Automation Letters*, vol. 7, no. 2, pp. 3695–3702, 2022.
- [18] J. Luo, P. Dong, Y. Zhai, Y. Ma, and S. Levine, "RLIF: Interactive imitation learning as reinforcement learning," in *The Twelfth International Conference on Learning Representations*, 2024. [Online]. Available: <https://openreview.net/forum?id=oLLZhbBSOU>
- [19] Y. Korkmaz and E. Btıyk, "Mile: Model-based intervention learning," 2025. [Online]. Available: <https://arxiv.org/abs/2502.13519>
- [20] P. Vitiello, K. Dreczkowski, and E. Johns, "One-shot imitation learning: A pose estimation perspective," in *7th Annual Conference on Robot Learning*, 2023. [Online]. Available: <https://openreview.net/forum?id=w5ONmpgnfG>
- [21] N. Heppert, M. Argus, T. Welschehold, T. Brox, and A. Valada, "Ditto: Demonstration imitation by trajectory transformation," in *2024 IEEE/RSJ International Conference on Intelligent Robots and Systems (IROS)*, 2024, pp. 7565–7572.
- [22] N. D. Palo and E. Johns, "Learning multi-stage tasks with one demonstration via self-replay," in *5th Annual Conference on Robot Learning*, 2021. [Online]. Available: <https://openreview.net/forum?id=p-TBwVowXRH>
- [23] J. Zhu, Y. Ju, J. Zhang, M. Wang, Z. Yuan, K. Hu, and H. Xu, "Densematcher: Learning 3d semantic correspondence for category-level manipulation from a single demo," in *The Thirteenth International Conference on Learning Representations*, 2025, spotlight. [Online]. Available: <https://openreview.net/forum?id=8oFvUBvF1u>
- [24] C. Tang, A. Xiao, Y. Deng, T. Hu, W. Dong, H. Zhang, D. Hsu, and H. Zhang, "Mimicfunc: Imitating tool manipulation from a single human video via functional correspondence," in *9th Annual Conference on Robot Learning*, 2025. [Online]. Available: <https://openreview.net/forum?id=CBYGhryESq>
- [25] A. Mandlkar, S. Nasiriany, B. Wen, I. Akinola, Y. Narang, L. Fan, Y. Zhu, and D. Fox, "Mimicgen: A data generation system for scalable robot learning using human demonstrations," in *7th Annual Conference on Robot Learning*, 2023. [Online]. Available: https://openreview.net/forum?id=dk-2R1f_LR
- [26] C. R. Garrett, A. Mandlkar, B. Wen, and D. Fox, "Skillgen: Automated demonstration generation for efficient skill learning and deployment," in *CoRL 2024 Workshop on Mastering Robot Manipulation in a World of Abundant Data*, 2024. [Online]. Available: <https://openreview.net/forum?id=mGqNcQY8ib>
- [27] J. Wang, Y. Qin, K. Kuang, Y. Korkmaz, A. Gurumoorthy, H. Su, and X. Wang, "Cyberdemo: Augmenting simulated human demonstration for real-world dexterous manipulation," in *2024 IEEE/CVF Conference on Computer Vision and Pattern Recognition (CVPR)*, 2024, pp. 17952–17963.
- [28] J. Yu, L. Fu, H. Huang, K. El-Refai, R. A. Ambrus, R. Cheng, M. Z. Irshad, and K. Goldberg, "Real2render2real: Scaling robot data without dynamics simulation or robot hardware," 2025. [Online]. Available: <https://arxiv.org/abs/2505.09601>
- [29] Z. Xue, S. Deng, Z. Chen, Y. Wang, Z. Yuan, and H. Xu, "Demogen: Synthetic demonstration generation for data-efficient visuomotor policy learning," in *7th Robot Learning Workshop: Towards*

Robots with Human-Level Abilities, 2025. [Online]. Available: <https://openreview.net/forum?id=TheehgB46p>

- [30] S. Levine, C. Finn, T. Darrell, and P. Abbeel, “End-to-end training of deep visuomotor policies,” *J. Mach. Learn. Res.*, vol. 17, no. 1, p. 1334–1373, Jan. 2016.
- [31] T. Z. Zhao, V. Kumar, S. Levine, and C. Finn, “Learning Fine-Grained Bimanual Manipulation with Low-Cost Hardware,” in *Proceedings of Robotics: Science and Systems*, Daegu, Republic of Korea, July 2023.
- [32] T. Ren, S. Liu, A. Zeng, J. Lin, K. Li, H. Cao, J. Chen, X. Huang, Y. Chen, F. Yan, Z. Zeng, H. Zhang, F. Li, J. Yang, H. Li, Q. Jiang, and L. Zhang, “Grounded sam: Assembling open-world models for diverse visual tasks,” 2024.
- [33] D. DeTone, T. Malisiewicz, and A. Rabinovich, “Superpoint: Self-supervised interest point detection and description,” in *Proceedings of the IEEE Conference on Computer Vision and Pattern Recognition (CVPR) Workshops*, 2018, pp. 224–236.
- [34] P. Lindenberger, P.-E. Sarlin, and M. Pollefeys, “Lightglue: Local feature matching at light speed,” in *Proceedings of the IEEE/CVF International Conference on Computer Vision (ICCV)*, 2023, pp. 17 627–17 638.
- [35] K. S. Arun, T. S. Huang, and S. D. Blostein, “Least-squares fitting of two 3-d point sets,” *IEEE Transactions on Pattern Analysis and Machine Intelligence*, vol. PAMI-9, no. 5, pp. 698–700, 1987.
- [36] M. A. Fischler and R. C. Bolles, “Random sample consensus: a paradigm for model fitting with applications to image analysis and automated cartography,” *Commun. ACM*, vol. 24, no. 6, p. 381–395, Jun. 1981. [Online]. Available: <https://doi.org/10.1145/358669.358692>
- [37] K. Shoemake, “Animating rotation with quaternion curves,” *SIGGRAPH Comput. Graph.*, vol. 19, no. 3, p. 245–254, Jul. 1985. [Online]. Available: <https://doi.org/10.1145/325165.325242>
- [38] J. Ho, A. Jain, and P. Abbeel, “Denoising diffusion probabilistic models,” in *Proceedings of the 34th International Conference on Neural Information Processing Systems*, ser. NIPS ’20. Red Hook, NY, USA: Curran Associates Inc., 2020.
- [39] S. James, Z. Ma, D. R. Arrojo, and A. J. Davison, “Rlbench: The robot learning benchmark & learning environment,” *IEEE Robotics and Automation Letters*, vol. 5, no. 2, pp. 3019–3026, 2020.
- [40] P. Wu, Y. Shentu, Z. Yi, X. Lin, and P. Abbeel, “Gello: A general, low-cost, and intuitive teleoperation framework for robot manipulators,” in *2024 IEEE/RSJ International Conference on Intelligent Robots and Systems (IROS)*, 2024, pp. 12 156–12 163.
- [41] R. Hoque, L. Y. Chen, S. Sharma, K. Dharmarajan, B. Thananjeyan, P. Abbeel, and K. Goldberg, “Fleet-Dagger: Interactive robot fleet learning with scalable human supervision,” in *Conference on Robot Learning (CoRL)*. PMLR, 2022, pp. 368–380.
- [42] S. G. Hart, “Nasa-task load index (nasa-tlx); 20 years later,” in *Proceedings of the human factors and ergonomics society annual meeting*, vol. 50, no. 9. Sage publications Sage CA: Los Angeles, CA, 2006, pp. 904–908.
- [43] S. G. Hart and L. E. Staveland, “Development of nasa-tlx (task load index): Results of empirical and theoretical research,” in *Human Mental Workload*, ser. Advances in Psychology, P. A. Hancock and N. Meshkati, Eds. North-Holland, 1988, vol. 52, pp. 139–183. [Online]. Available: <https://www.sciencedirect.com/science/article/pii/S0166411508623869>
- [44] W. J. Conover, *Practical nonparametric statistics*. john wiley & sons, 1999.

TABLE VI: Simulation Hyper-parameter

Main Hyper-param.	Value
Image type	Wrist
Proprioceptive input	Joint angle
Action output	Delta EE pose
Image encoder	ResNet-18
Optimizer	AdamW
Learning rate	1e-4
Weight decay	1e-6
Batch size	64
DP Hyper-param.	Value
H^p	8
H^{exec}	4
H^{obs}	2
Diff. step embed. dim.	64
U-net dims.	[64, 128, 256]
LSTM/GMM Hyper-param.	Value
mode num.	5
lstm dim.	1032
lstm layer num.	2
sequence length	10

APPENDIX

A. Hyperparameter Settings

The hyperparameter (Hyper-Param.) settings for end-to-end IL policies, namely diffusion policy, BC-RNN, and CNN-GMM, are shown in the Table VI. For real-world experiments, only the diffusion policy is utilized, and its action output is changed to the joint angle.

B. Algorithm of Data Collection Strategy

Algorithm 2 Algorithm of Data Collection Strategy

```

function DEPLOY( $\pi^H, \pi^A, \pi^N, \text{Num}, \text{Label}, \beta$ )
   $\mathcal{D}' \leftarrow \emptyset, \mathcal{W}' \leftarrow \emptyset$ 
  for  $i = 1$  to Num do
    Init. env. as  $o_0, x_0, \tau_i \leftarrow \emptyset, w_i^\tau \leftarrow \emptyset, j \leftarrow 0, k \leftarrow 0,$ 
     $\text{Done} \leftarrow \text{False}$ 
    while Not Done do
      if  $\text{mod}(j, H) = 0$  then
         $X_j \sim \mathcal{U}(0, 1)$ 
      else
         $X_j \leftarrow X_{j-1}$ 
      end if
      if Human intervenes then
         $h(k) \leftarrow 1$ 
      else
         $h(k) \leftarrow 0$ 
      end if
      if  $X_j < \beta$  or  $x_k \in \mathcal{B}$  then
         $g(j, k) \leftarrow 1$ 
      else
         $g(j, k) \leftarrow 0$ 
      end if
      if  $\text{Label} == \text{ONE\_DEMO}$  then
         $a_k \leftarrow \pi^H(x_k)$ 
      else if  $\text{Label} == \text{REST\_DEMO}$  then
        if  $h(k) == 1$  then
           $a_k \leftarrow \pi^H(x_k)$ 
        else
           $a_k \leftarrow \pi^A(o_k)$ 
        end if
      else if  $\text{Label} == \text{CORRECTION}$  then
        if  $h(k) == 1$  then
           $a_k \leftarrow \pi^H(x_k)$ 
        else if  $g(j, k) == 1$  then
           $a_k \leftarrow \pi^A(o_k)$ 
           $j \leftarrow j + 1$ 
        else
           $a_k \leftarrow \pi^N(o_k)$ 
           $j \leftarrow j + 1$ 
        end if
      end if
      end if
       $\tau_i \leftarrow \tau_i \cup \{(o_k, a_k)\}$ 
      if  $a_k$  is from  $\pi^H(x_k)$  or  $\pi^A(o_k)$  then
         $w_i^\tau \leftarrow w_i^\tau \cup \{1\}$ 
      else
         $w_i^\tau \leftarrow w_i^\tau \cup \{0\}$ 
      end if
       $o_{k+1}, x_{k+1}, \text{Done} \leftarrow \text{env.step}(a_k)$ 
       $k \leftarrow k + 1$ 
    end while
     $\mathcal{D}' \leftarrow \mathcal{D}' \cup \{\tau_i\}, \mathcal{W}' \leftarrow \mathcal{W}' \cup \{w_i^\tau\}$ 
  end for
  return  $\mathcal{D}', \mathcal{W}'$ 
end function

```
